Enhancement and anticipation of the Ioffe-Regel crossover in amorphous/nanocrystalline composites. Supplementary Material

A. Tlili,[1] V. M. Giordano,[2] Y. M. Beltukov,[3] P. Desmarchelier,[4] S. Merabia,[2] and A. Tanguy[4,1]

[1] *Université de Lyon, LaMCoS, INSA-Lyon, CNRS UMR5259, F-69621, France*
[2] *Institut Lumière Matière, UMR 5306 Université Lyon 1-CNRS, F-69622 Villeurbanne Cedex, France*
[3] *Ioffe Institute, 194021 St. Petersburg, Russian Federation*
[4] *LaMCos, INSA-Lyon, CNRS UMR5259, Université de Lyon, F-69621 Villeurbanne Cedex, France*

PACS numbers: 61.43.Dq, 61.43.Fs, 63.50.-x, 65.60.+a, 62.20.-x

I. SPATIALLY RESOLVED DENSITY OF STATES

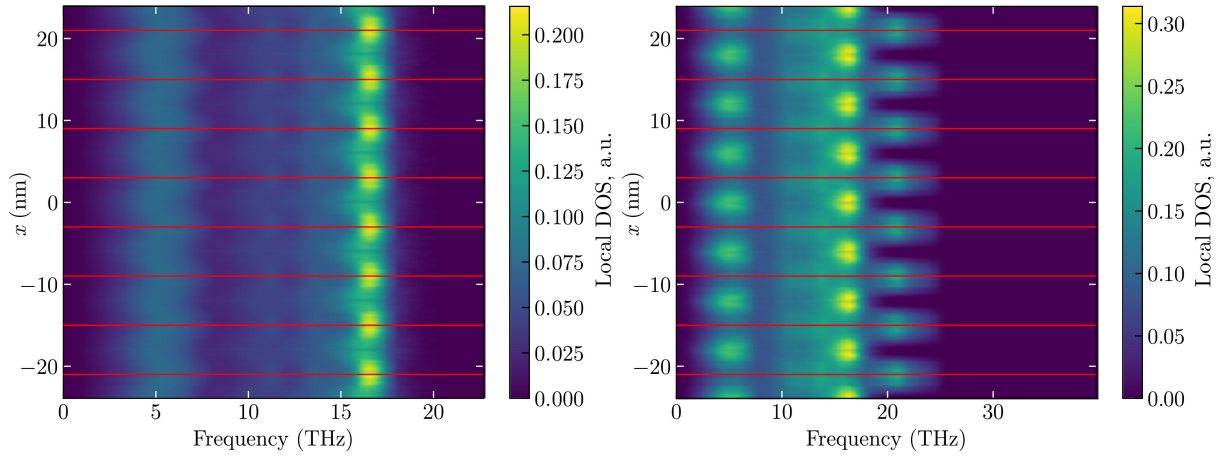

FIG. 1: Spatially resolved vibrational density of states in the system $\chi = 1$ (left) and $\chi = 4.6$ (right). Horizontal lines mark the position of the inclusions.

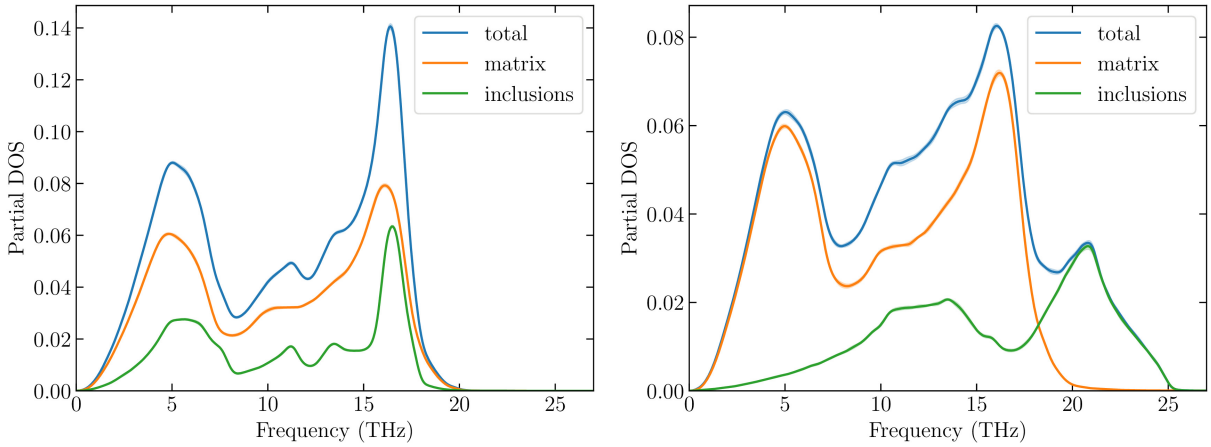

FIG. 2: Density of states calculated for only atoms within the matrix (red), the inclusion (green) and all atoms (blue) for the nanocomposites with $\chi = 1$ (left) and $\chi = 4.6$ (right). The high energy modes in the high elastic contrast system is clearly due to the presence of higher energy vibrations in the hard inclusion.

Another insight can be obtained by looking to the spatially resolved DOS, in Fig. 1: here we report for the systems without (a) and with (b) elastic contrast the local DOS calculated for different positions along the x direction, i.e. the DOS corresponding to atoms with a given value of x, with a spatial resolution 1.6 Å.

For the $\chi = 1$ sample, we observe a modulation of the intensity of the two maxima at 6 and 16 THz, with a maximum intensity at the nanoinclusions positions, corresponding to the sharper density of states in the crystalline system with respect to the fully amorphous one. In the case of the $\chi = 4.6$ sample, the situation is more intriguing. Due to the DOS renormalization, we observe a weakening of these maxima within the nanoinclusions, so that almost only the high energy crystalline specific modes, for $\omega \geq 18$ THz, are clearly visible. It results then that modes for $\omega \leq 18$ THz are globally localized in the amorphous matrix, while modes for $\omega \geq 18$ THz are clearly localized in the inclusions. We notice here that we are not talking of Anderson localization, but of modes which imply mostly atoms in the matrix or in the inclusions.

To confirm this picture, we can look at the projection of the DOS onto the different components of the nanocomposite, and calculate the DOS corresponding only to atoms in the inclusions and only to atoms in the matrix. This is shown in Figure 2. For the $\chi = 1$ sample, both components of the DOS have a similar form but the DOS of the amorphous matrix is more broadened. As a result, frequencies in the tail above 18 THz belongs to the amorphous matrix only. However, for the $\chi = 4.6$ sample, the DOS of crystalline inclusions is shifted towards higher frequencies, with the arising of a broad peak in the 18–25 THz region, due to the high energy optic modes.

II. POLARIZATION PROJECTED DENSITY OF STATES

In order to calculate the propagative part of the thermal conductivity, we had to distinguish between longitudinal and transverse polarization, which differ by the different sound velocity, acoustic dispersion, mean free path and density of states. While the former have been directly obtained with the molecular dynamics simulations, getting the longitudinal and transverse projected density of states is not trivial in a disordered system because of the ill-definition of the notion of wave vector. Therefore, we have used the method of Voronoi cells to calculate such projections[1,2]. In this method, we find the Voronoi cell volume around each atom. For any atomic displacement u, we can find the transverse component $u_T = \mathcal{P}_T u$, which does not change the Voronoi cell volume. The remaining part $u_L = u - u_T = \mathcal{P}_L u$ is the longitudinal component. Figure 3 shows the decomposition of the DOS $g(\omega) = g_L(\omega) + g_T(\omega)$ calculated by using the Kernel Polynomial Method with projection operators $\mathcal{P}_L$ and $\mathcal{P}_T$[1]. In the low-frequency region (below ~ 7 THz),

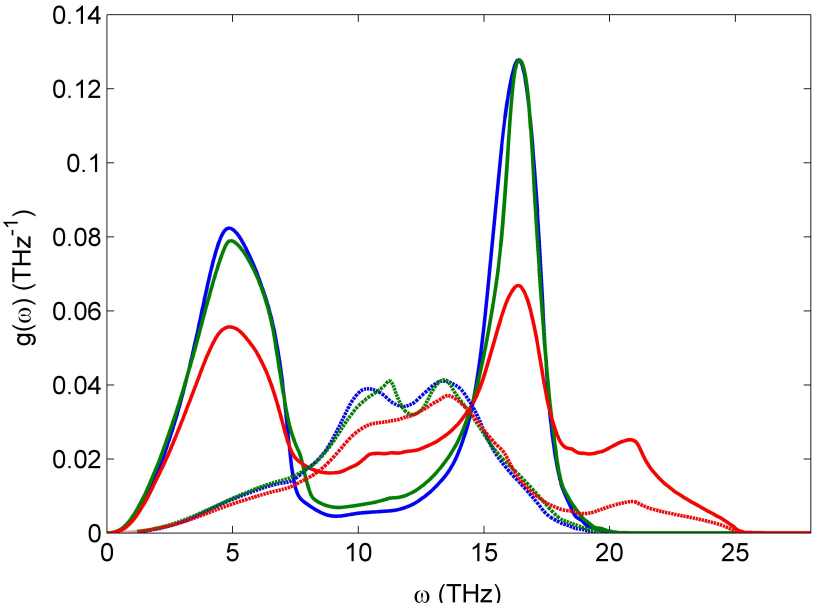

FIG. 3: Density of states projected on the transverse (solid line) and longitudinal (dashed line) polarizations for the fully amorphous (blue), the $\chi = 1$ (green) and the $\chi = 4.6$ (red) samples.

the transverse modes dominate the DOS. However, at 7 THz there is a sharp transition from mostly transverse modes to mostly longitudinal ones. It corresponds to the maximum frequency (8 THz) of TA modes in crystalline silicon. The high-frequency region (above 15 THz) is mostly transverse, which corresponds to TO modes in crystalline silicon. However, these modes do not contribute to the thermal conductivity, being close to the mobility edge.

III. MEAN FREE PATH

From the kinetic energy envelope of the traveling wavepackets, it is possible to extract the mean free path by fitting the propagative part with the Beer-Lambert law. The so calculated mean free paths for the fully amorphous system and the two composites are reported in Fig. 4 for both polarizations. The impact of the nanostructuration is evident: for both polarizations the mean free path is reduced by almost one order of magnitude. This is the major effect, while only a reduction of less than a factor of two is obtained for an elastic contrast increased by almost a factor of 5.

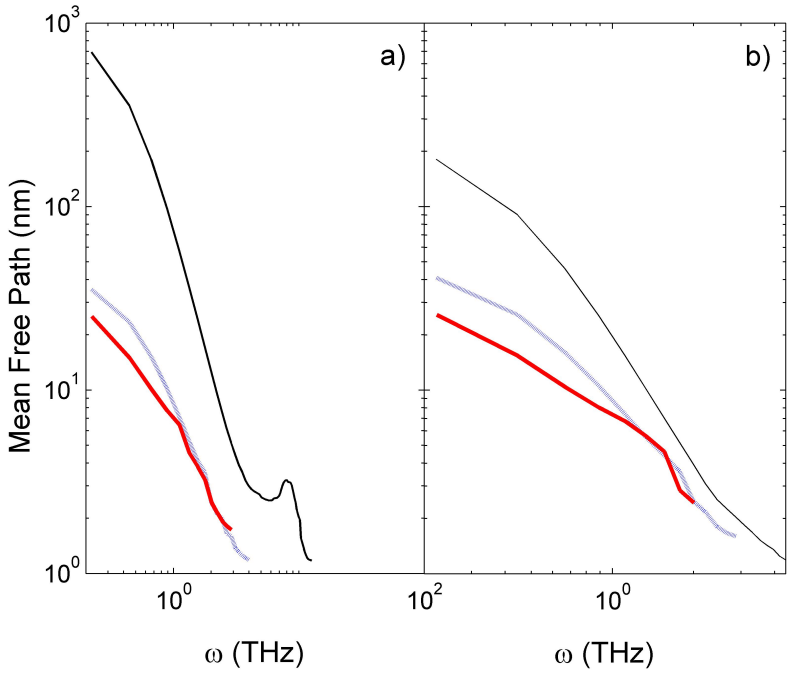

FIG. 4: Mean free path as obtained by the exponential fit of the kinetic energy envelope below the Ioffe-Regel limit for the longitudinal (a) and transverse (b) polarization and the fully amorphous system (thin black line), the nanocomposite $\chi = 1$ (dotted blue line) and $\chi = 4.6$ (thick solid red line).

A. Long mean free path and calculation of the propagative contribution to the thermal conductivity

The low energy phonons have quite long mean free path, which could raise the question about a good estimation of their contribution to the thermal conductivity.

Concerning the calculation of the thermal conductivity using the microscopic dynamics and the integral formulas for the propagative and diffusive parts, the mean free paths considered here are smaller than the size of the global simulation box used to study wave packets transportation, from which the mean free path has been deduced. The propagative contribution to thermal conductivity is thus well estimated. Concerning the calculation of the thermal conductivity, using the Green-Kubo formula, this calculation has been performed using equilibrium simulations with periodic boundary conditions. These types of boundary conditions do not affect the dynamics of mean free paths larger than the box size, see Ref.[3] for a discussion of this point. By contrast, non-equilibrium simulations involving thermostats would scatter propagons having mean free paths larger than the box size. Employing equilbrium Green-Kubo simulations in combination with periodic boundary conditions ensures that this scattering phenomenon does not occur Therefore, the contribution from propagons is not underestimated in our Green-Kubo calculations.

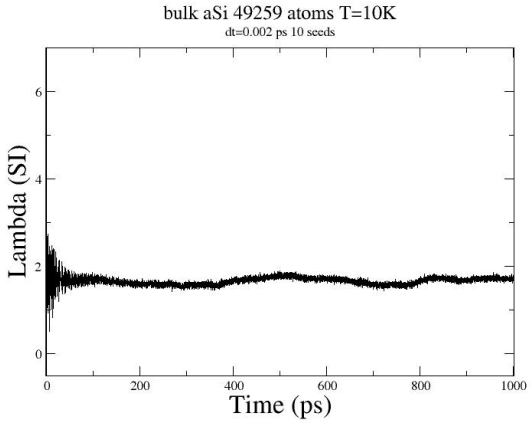

FIG. 5: We report here the thermal conductivity (lambda) as a function of time of the simulation as obtained in a bulk amorphous sample at 10 K.

IV. CONVERGENCE OF THERMAL CONDUCTIVITY CALCULATIONS WITH THE GREEN-KUBO METHOD

As mentioned in the main text, we report in the manuscript results from simulations 0.25 ns long. Before choosing this time length, we have run simulations up to 1000 ps long. In Fig 5 the calculation of the thermal conductivity in a fully amorphous sample at 10 K is reported, clearly showing that the plateau of the thermal conductivity is well defined and the calculation has converged for shorter times, such as 250 ps. It is to be noticed that the amorphous system is the one with the smallest thermal conductivity, which means that the result is most sensitive to the noise. We have run such long simulations for all systems and deliberately chosen to analyze only the first 250 ps, as it is known that in disordered systems, for long times the noise in the correlation function tends to produce a large numerical uncertainty[4]. For this reason, it is better suited and more efficient to average over independent simulations more than running long simulations[5], which is what we have chosen to do. Finally, we notice that 250 ps is a reasonable time, where calculations have converged, the plateau is well distinguishable and it is a larger time than the longest phonon lifetime in amorphous silicon (100 ps for 1 THz excitation)

V. WAVE-PACKET PROPAGATION

As shown in the main text, the introduction of nanoinclusions causes an anticipation of the propagative to diffusive crossover in the wave-packet propagation. Here we report the space-time-vibrational kinetic energy $(x-t-E)$ map of longitudinal wave-packets propagating in the fully amorphous system and in the two nanocomposites with $\chi = 1$ and with $\chi = 4.6$ elastic contrast. Wave-packets of the same amplitude have been generated in the center of the systems, within the nanoinclusions in the nanocomposites, and their propagation has been followed in time.

In this representation, a straight line in the $x - t$ space corresponds to a propagative mode whose velocity is given by its slope. When propagative and diffusive characters coexist (around the Ioffe-Regel crossover), atoms incoherently vibrate after the propagative wave-front has passed. This reflects into the arising of some intensity for distances below the one of the traveling wave, and remaining at all times. In the fully diffusive regime (higher frequency) the intensity remains localized around the starting point with a spacial width which only for short times increases linearly, but then only expands as a squareroot of time.

We report here four frequencies: 0.5, 1.55, 8.9 and 15 THz. The first and the last, reported in Fig. 6 lie well below and well above the Ioffe-Regel crossover for all samples. Here the behaviors are quite similar, clearly showing a fully propagative and a fully diffusive regime.

The other two frequencies mark different behaviors and are reported in Fig. 7: $\nu = 1.55$ THz corresponds indeed to the crossover only for the $\chi = 4.6$ sample, while $\nu = 8.9$ THz is still below Ioffe-Regel for the amorphous system. Looking to the maps at $\nu = 1.55$ THz, it is clear that a weak diffusive contribution is already present in the amorphous sample, with some intensity remaining behind the front wave, still following it. In the nanocomposites the intensity starts to be more and more concentrated in a narrow region close to the starting position, at all times. While this is still associated with a propagating front wave in the $\chi = 1$ sample, in the $\chi = 4.6$ sample the propagating front wave is extremely weak and disappearing, indicating that we are crossing the Ioffe-Regel condition.

At $\nu = 8.9$ Tz, the propagative to diffusive transition is terminated for both nanocomposites. This is not true for the amorphous sample, where a weak propagative part is still visible. Indeed the Ioffe-Regel crossover for longitudinal waves is at 12.7 THz in the amorphous.

Comparing the three samples at all frequencies, the anticipation of a mixed propagative-diffusive character and of the Ioffe-Regel crossover in the nanocomposites can be clearly appreciated.

[1] Y. Beltukov, C. Fusco, D. Parshin, and A. Tanguy, Phys. Rev. E **93**, 023006 (2016).
[2] Y. Beltukov, C. Fusco, A. Tanguy, and D. Parshin., J. Phys.: Conf. Ser. **661**, 012056 (2015).
[3] K. Termentzidis and S. Merabia, eds., *Molecular Dynamics Simulations and Thermal Transport at the Nano-Scale* (Intech Open Access, 2012).
[4] J. Barrat and F. Chiaruttini, Mol. Phys. **101**, 1605 (2003).
[5] K. Esfarjani, G. Chen, and H. Stokes, Phys. Rev. B **84**, 085204 (2012).

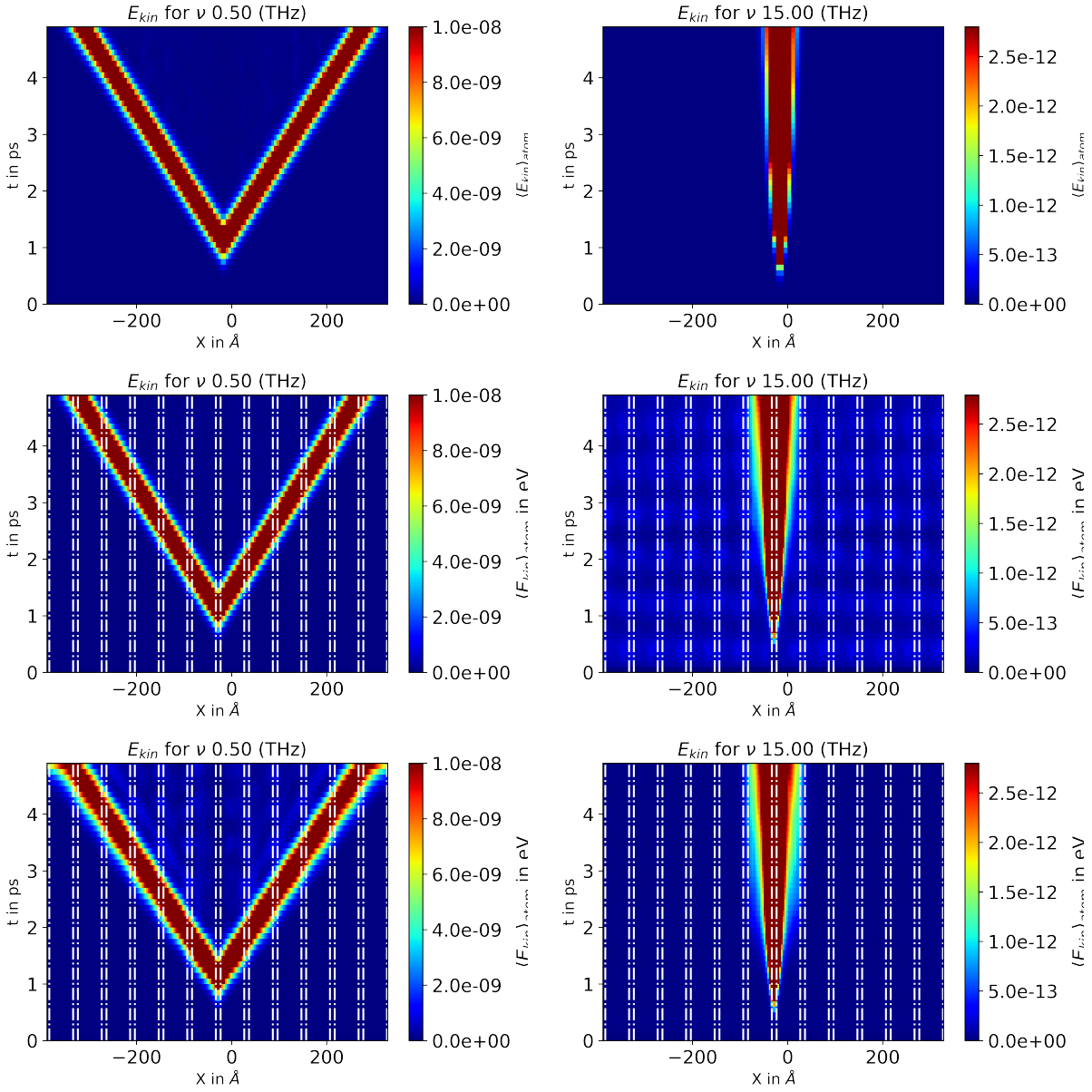

FIG. 6: First, Second and Third raw: Amorphous, $\chi = 1$ and $\chi = 4.6$ samples respectively. Dashed vertical lines in the nanocomposites identify the position of the nanoinclusions: here the wave-packet has been generated between two nanoinclusions.The color scale is the same for all samples for a given frequency, and is indicated on the right: it represents the vibrational kinetic energy of the atoms. At $\nu = 0.5$ THz (left) the regime is clearly propagative for all samples, with a linear dependence of the front wave position with respect to time. At $\nu = 15$ THz (right), we are above Ioffe-Regel in all samples. The regime is clearly fully diffusive, with a kinetic energy which slowly expands from the starting point as the squareroot of time.

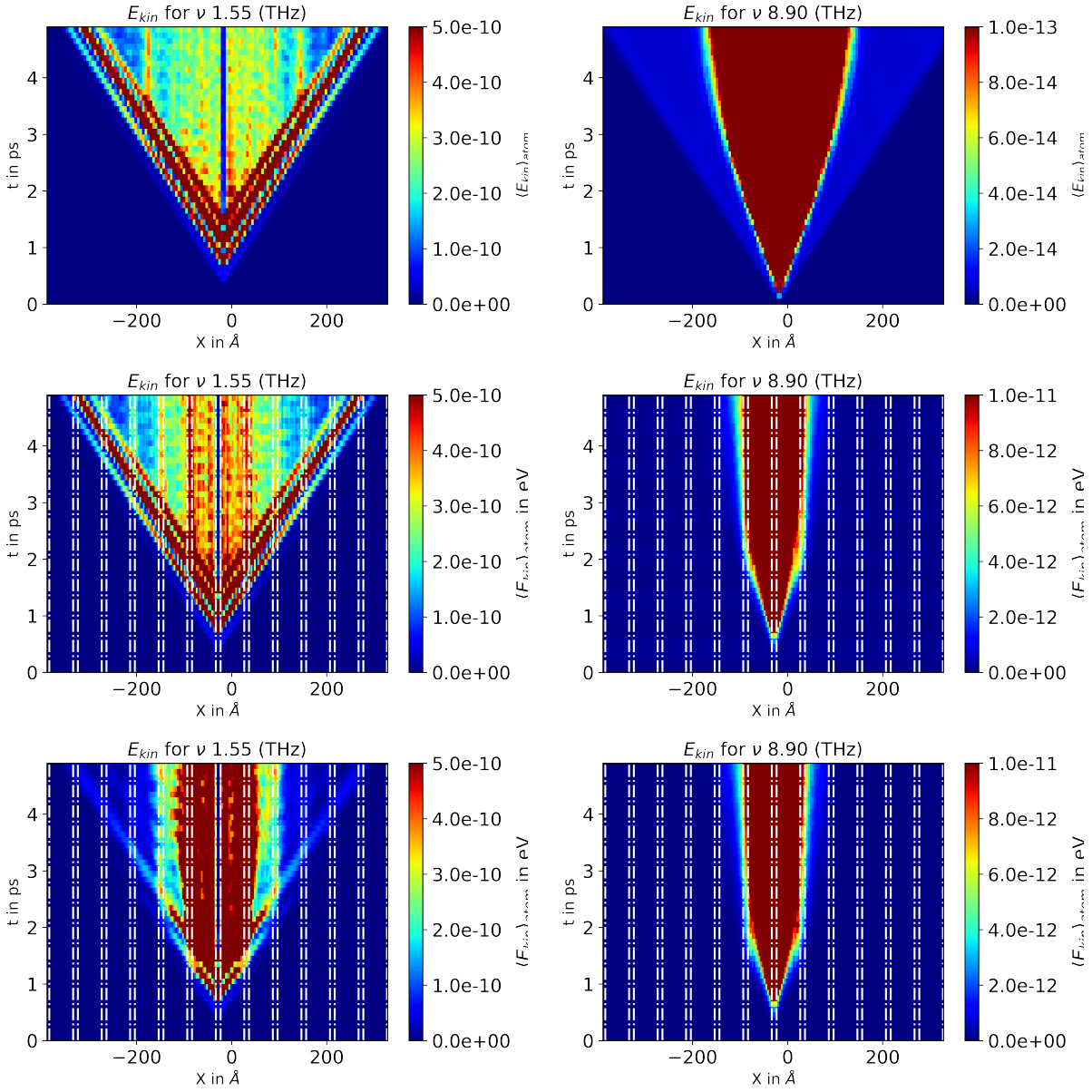

FIG. 7: First, Second and Third raw: Amorphous, $\chi = 1$ and $\chi = 4.6$ samples respectively. Dashed vertical lines in the nanocomposites identify the position of the nanoinclusions: here the wave-packet has been generated between two nanoinclusions.The color scale is the same for all samples for a given frequency, and is indicated on the right: it represents the vibrational kinetic energy of the atoms. At $\nu = 1.55$ THz (left) the regime is clearly of mixed propagative and diffusive caracter in the nanocomposites. For $\nu = 8.9$ THz (right), the color scale for the amorphous sample has been enhanced in order to highlight the presence of a propagative front, which is absent in the nanocomposites, where the regime is finally fully diffusive.